HYDROGEN PHOTO-PRODUCTION FROM GLYCEROL ON PLATINUM, GOLD AND SILVER-MODIFIED TiO_2-USY62 CATALYSTS

Francisco J. López-Tenllado[a], Rafael Estévez[a], Jesús Hidalgo-Carrillo[a,*], Silvia López-Fernández[a,1], Francisco José Urbano[a] and Alberto Marinas[a]

[a]*Departamento de Química Orgánica, Instituto Universitario de Investigación en Química Fina y Nanoquímica (IUNAN), Universidad de Córdoba, E-14071 Córdoba, Spain*

Abstract

In this work, photocatalysts consisting of TiO_2 supported on zeolite (USY62) were synthesized by sol-gel method and, subsequently, a noble metal (Pt, Au, or Ag) was incorporated by impregnation or photodeposition. Zeolite-TiO_2 composites were characterized by SEM, TEM, XRD, N_2 adsorption-desorption, Raman and UV–vis spectroscopy, and well-dispersed anatase TiO_2 particles (ca. 10 nm) that exhibited a blue-shift in the UV–vis absorption due to the size quantization effect were produced. The photocatalytic activity of all zeolite-TiO_2 composites was examined by the photoreforming of aqueous glycerol solution (10% w/w) under UV and solar-simulated radiation. The activity of the zeolitic photocatalysts decreased in the order Pt > Au > Ag, being catalysts prepared by photodeposition more active than those prepared by impregnation. Moreover, Zeolite-supported TiO_2, led to a TiO_2 with smaller deactivation in H_2 production than unsupported TiO_2, which can be ascribed to the small TiO_2 particle size or an interaction zeolite-TiO_2. All

[1] Present address: Rovi CM, Juan Camarillo 35, E-28037 Madrid, Spain

* Corresponding author. Tel: +34957218622 E-mail addresses: q12hicaj@uco.es (Jesús Hidalgo-Carrillo)

in all, a photocatalyst (USY-Ti-PPt) with TiO_2 up to four times more active than unsupported TiO_2 under UV radiation was prepared.

Keywords

Photocatalysis, Photoreforming, Hydrogen production, Zeolite, TiO_2, Photodeposition

1. Introduction

Nowadays, the energetic system is largely based on non-renewable sources such as fossil fuels, coal, oil, and natural gas, which represent more than 80 % of the primary energy. The economic and environmental concern is increasing the interest in the search for alternative and sustainable fuels. Hydrogen is regarded as a promising alternative as energy vector, since it has an energetic value of 122 kJ/g, which is higher than the majority of fossil fuels, and its combustion produces exclusively water as a byproduct, that is, no emission of toxic substances or greenhouse gases during combustion [1].

In contrast with carbon, petrol, or natural gas, hydrogen is the most abundant element of the universe, but it cannot be found as molecular hydrogen in the earth. Therefore, hydrogen is not a natural resource, that is to say, it cannot be obtained by a direct way but some transformations are necessary which require energy consumption, nuclear, fossil or renewable. The most widespread methodology for hydrogen production is the steam reforming of hydrocarbons, a non-renewable feedstock, with water. Hence, 48 % of production comes from the reforming of natural gas, 30 % from the reforming of oil, and 18 % from the reforming of carbon. Finally, 4 % of hydrogen production is due to water electrolysis [2].

An alternative to produce hydrogen is the utilization of biomass, which is a renewable source derived from plant and animal wastes since the carbon dioxide emissions from these sources belong to the carbon cycle. There are some innovative techniques for sustainable hydrogen production using biomass, such as the use of organisms that could produce it under specific conditions [3], pyrolysis, steam reforming, and steam gasification [4] or photocatalytic reforming of organic oxygenated compounds [5].

Semiconductors, which are normally used as photocatalysts in photocatalytic reforming, can absorb a photon of light to excite an electron from the valence band to the conduction band, exceeding the prohibited energy, and leaving a positively charged hole in the valence band. Photoinduced holes (h+) are oxidizing agents in the deprotonation of water and oxygenated organic compounds, while photoinduced electrons (e^-) reduce protons to molecular hydrogen [6]. TiO_2 is one of the most used photocatalysts in this type of reaction, due to its availability, chemical stability, price, and photocorrosion resistance [7]. However, TiO_2 has some drawbacks such as the rapid recombination of electron-hole pairs, where about 90% or more of the photogenerated electrons recombine in 10 ns [8], low surface area, limited light absorption, high agglomeration tendency, and high light scattering that obstructs the light from reaching active sites on catalyst surface [9].

Several modifications have been used to overcome these limitations such as the addition of electron donors, the doping with metal ions, the sensitization with dyes, the formation of heterojunction with other semiconductors, or the loading of metals, among others [10]. The loading of metals as co-catalysts of TiO_2 can affect in different ways, such as displacing the absorption region of UV to visible light due to the d orbitals of the metals decreasing the

prohibited energy gap (Eg), increase the light absorption favored by the surface plasmon resonance of the electrons of the metals [11], act as electron traps and reducing the recombination of electron-hole pairs, and they can favor the production of hydrogen [7]. For this purpose, noble metals, especially platinum, are considered the most active cocatalysts in the field of hydrogen photoproduction.

Moreover, the dispersion of the photocatalyst on a support could inhibit the growth of crystallite sizes and avoid the aggregation of the semiconductor [9]. Among the different supports, zeolites have been considered a good option due to their high surface area, hydrophobicity/hydrophilicity, adsorption capacity, stability [12], and electron donors and acceptors capacities [13]. Additionally to the dispersion effect, it has been found that the exceptional adsorptive capacity of zeolite can be used to enrich the pollutants concentration around TiO_2, and enhance the photocatalytic degradation of VOCs [14], dyes [15–17], pesticides [18] or SO_2 [19], among others.

Regarding the preparation of TiO_2-zeolite composites, researchers have taken advantage of the ordered structure of zeolites, which cannot only act as adsorbers but also provide sites to enhance the interaction of zeolite-TiO_2, being the sol-gel method the most common procedure to synthesize the composite due to the ease of the procedure [15,20,21].

In addition to the degradation of pollutants, there are some other examples in the literature on the use of Zeolite-TiO_2 composites in photocatalysis. Therefore, for instance, such composites have been described to lead to an increase in the conversion of glucose to acids [22,23]. Other researchers carried out the photocatalytic production of Hydrogen with Zeolite-TiO_2-Co systems acting the zeolite as an electron acceptor [24,25], and Zeolite-TiO_2-

Au systems acting the zeolites as a molecular sieve [26]. Nevertheless, there is still much to investigate in the photocatalytic production of hydrogen with zeolite-TiO_2 systems.

In the present study, we prepared several USY-TiO_2-metal (Pt, Au, and Ag) composites and tested them in the photocatalytic production of hydrogen from glycerol. Firstly, TiO_2 was supported on USY by the sol-gel method and metal was subsequently incorporated by impregnation or photodeposition.

2. Materials and methods

2.1 Catalyst preparation

All solids were synthesized by using a USY zeolite (Si/Al ratio 62) as the support. Titanium was incorporated using titanium isopropoxide (Sigma-Aldric, ref. 205273) as the precursor in order to have a nominal content of 14% TiO_2 by weight in the resulting material. Therefore, 10 g of zeolite previously treated at 400 ºC in air flow for 4 h was introduced in a 250 mL round-bottom flask together with 60 mL of propan-2-ol 99.5% (Sigma-Aldric, ref. 190764) and 6.14 mL titanium isopropoxide 97% (Sigma-Aldric, USA). The mixture was heated at ca. 90 ºC (propan-2-ol reflux) for 14 h. Then, a solution of 322.5 mg dipicolinic acid (Sigma-Aldric, ref. 61905) in a mixture of 20 mL propan-2-ol and 2.5 mL water was added to favor the formation of the gel and the mixture was kept under reflux for two more hours. The solid was then vacuum-filtered and washed with 10 mL of propan-2-ol three times. Finally, the system was calcined at 550ºC for 4 h in static air thus resulting in the solid being labelled as USY-Ti.

Incorporation of the noble metals (Au, Pt, or Pt) was made through photodeposition or impregnation at a nominal value of noble metal/Ti 0.1 by weight (i.e., 10% w/w). Ag(acac) (Sigma Aldrich, ref. 323489), $Pt(acac)_2$ (Fluka art. 81030), and $KAuCl_4$ (sigma Aldrich, ref. 334545), were used as the metal precursors.

Impregnation: a mixture containing 1.5 g of catalyst and the appropriate amount of the metal precursor dissolved in 400 mL propan-2-ol was introduced in a round-bottom flask. The mixture was stirred gently (1000 rpm) and the solvent was rotavaporated. The solid was resuspended in 50 mL propan-2-ol, filtered, and washed several times with the same solvent. Finally, it was calcined at 550ºC for 4h under static air. The solids thus obtained were labelled as USY-Ti-IAg, USY-Ti-IPt, and USY-Ti-IAu referring to the method (I stands for impregnation) and the incorporated metal (silver, platinum, or gold, respectively).

Photodeposition: a mixture of 1.5 g USY-Ti catalyst and the appropriate amount of the metal precursor dissolved in propan-2-ol was introduced in the photochemical reactor (Photochemical Reactors LTD, Model 3010). The mixture was stirred in the dark at 1000 rpm for 20 min in order to reach adsorption equilibrium. The mixture was then submitted to the light (125 W mercury lamp, λ = 365 nm, $1.2 \cdot 10^{-5}$ Einstein$\cdot s^{-1}$ as measured through ferrioxalate actinometry) for 2 h. Temperature was controlled at 20ºC. The solid was then vacuum-filtered, washed with propan-2-ol, and calcined at 550ºC for 4 h under static air. The solids thus obtained were named USY-Ti-PAg, USY-Ti-PPt, or USY-Ti-PAu depending on the metal incorporated through photodeposition being silver, platinum, or gold, respectively. Additionally, a TiO_2-Pt catalyst (0.5% w/w) was also prepared through the photodeposition method to compare the catalytic activity of our zeolitic photocatalysts. TiO_2 P25 Degussa

(Evonik, Germany) was used as titania support and the same photodeposition procedure described above was followed with a calcination temperature of 550ºC.

2.2 Characterization

Elemental analyses of the samples by inductively coupled plasma mass spectrometry (ICP-MS) were performed by the staff at the Central Service for Research Support (SCAI) of the University of Córdoba. Measurements were made on a Perkin–Elmer ELAN DRC-e instrument and, prior analysis, samples were dissolved with a H_2SO_4:HF:H_2O (1:1:1) mixture. Additionally, the metallic content (Au, Ag, and Pt) of the sample was determined by X-ray fluorescence analysis. Measurements were made on a Rigaku tube-above wave-length dispersive X-ray fluorescence ZSX Primus IV spectrometer, equipped with an X-ray tube with 4 kW rhodium anode, a proportional gas flow detector for light elements, and a scintillation counter for heavy elements.

The textural properties of solids were determined from N_2 adsorption-desorption isotherms (77K) by using a Micromeritics ASAP-2010 instrument. Surface area was calculated by the BET method, while pore distribution was determined by the BJH method. The samples (~0.1 g) were degassed at 473 K under vacuum (0.1 Pa) for 8 h prior to adsorption experiments.

XRD spectra of all catalysts were performed on a Siemens D-5000 X-Ray diffractometer provided with an automatic control and data acquisition system (DACO-MP). Analyses were performed with a nickel-filtered copper radiation (l = 1.5406 A) at 40 kV and 30 mA. Scans were performed at 0.02° 2θ intervals over the 2θ range from 2 to 85° at a rate of $2°\cdot min^{-1}$.

Raman spectra were obtained on a Perkin-Elmer 2000 NIR FT-Raman system with a Nd:YAG laser (1064 nm, 300 mW). It was operated throughout the 3600-200 cm^{-1} range at a resolution of 4 cm^{-1} and 64 scans.

Diffuse reflectance UV–Vis spectra were performed on a Cary 1E (Varian) spectrophotometer, using barium sulphate as reference material. Band gap values were obtained from the plot of the modified Kubelka–Munk function $[F(R)\cdot E]^{1/2}$ versus the energy of the absorbed light. Extrapolation to y = 0 of the linear regression in the 3.5–3.8 eV range afforded the band gap value.

FT-IR spectra were performed on a Bomen MB-100 FT-IR spectrophotometer. The pellets were prepared by mixing the solid with KBr in a 5:95 (w/w) ratio and recorded over a wavenumber range 400-4000 cm^{-1}.

2.3 Photocatalytic reaction

Experiments under UV light were performed in a Pyrex cylindrical doubled-walled immersion reactor (23 cm long×5 cm internal diameter, with a total volume of 190 cm^3) with a medium pressure 125 W Hg lamp supplied by Photochemical Reactors Ltd as the excitation source. 65 mg of catalyst was added to 65 mL of glycerol (Sigma-Aldric, ref. G9012) solution (10% v/v in water). All through the process, Ar was bubbled through the suspension (20 $mL\cdot min^{-1}$), and outlet gas composition was on-line analyzed during 16 hours by mass spectrometry, H_2 (m/z = 2) and CO_2 (m/z = 44) being calibrated with 2% H_2 and 1% CO_2 in Ar flows, respectively.

Simulated solar light (Newport, Xe lamp, $1.9 \cdot 10^{-7}$ Einstein$\cdot s^{-1}$ as measured through ferrioxalate actinometry) experiments were performed in a closed Pyrex cylindrical vessel (20 mL). 10 mg of catalyst was dispersed into 10 mL of glycerol solution (10% v/v in water). In a typical experiment, reaction was performed under an inert atmosphere, achieved by bubbling an Ar flow (20 mL$\cdot min^{-1}$) for 30 min. The catalyst suspension was continuously stirred (800 rpm), the reactor was thermostated at 20°C, and the glycerol solution was directly irradiated for 3 hours with the solar-simulated light.

Analyses were performed by sampling 1 mL from the head space of the photoreactor with a pressure-lock precision analytical syringe (Valco VICI Precision Syringes, 1 mL, leak-tight to 250 psi). Samples were analyzed by gas chromatography with a thermal conductivity detector (GC-TCD) on an Agilent Technologies 7890A gas chromatograph furnished with a Supelco Carboxen 1010 Plot column. Injector temperature was set at 150°C and detector at 250°C. Nitrogen was used as the carrier gas at 20 mL$\cdot min^{-1}$ (4 psi, 0.7 mL$\cdot min^{-1}$ through the column). The oven temperature was kept at 70°C for 2 min, then ramped up to 120°C at 10°C$\cdot min^{-1}$, and the final temperature was kept for 13 min.

3 Results and Discussion

3.1. Characterization of the photocatalysts

X-ray diffraction profiles of the samples are shown in Fig. 1. According to the diffraction patterns, the crystalline framework of Y-type zeolite (USY) [27] was present in the original zeolite and its structure was maintained after the incorporation of TiO_2 and the deposition of the metals. As far as USY-Ti-X systems are concerned, XRD spectra hardly show diffraction

peaks of anatase TiO_2 which suggests that either the TiO_2 content is low, or it has a small crystal size. The TiO_2 content was analyzed by ICP-MS and the results are shown in Table 1. TiO_2 content in Ti-USY-X systems was in the 12.0-14.4% (w/w) range; therefore, low TiO_2 crystal size is expected in the solids. Moreover, the broadening of the diffraction peak at $2\theta = 25.3^o$ (101 of anatase) suggests a good dispersion of the TiO_2 on the zeolite.

Regarding the systems with noble metal, USY-Ti-IAu and USY-Ti-PAu had intense diffraction peaks at $2\theta = 38.2^o$ (111) and $2\theta = 44.4^o$ (200) due to the metallic Au, which suggests the presence of big particles of Au in our systems. Ag and Pt systems did not show reflection peaks at $2\theta = 38.1^o$ and $2\theta = 39.8^o$, related to Ag and Pt respectively, which suggests a small crystallite size for Ag and Pt in our catalysts since the Ag and Pt content in the catalysts was ca. 1% w/w.

Raman spectra of USY and USY-Ti are shown in Fig. 2a. TiO_2 containing samples had three peaks centered at 399, 518, and 640 cm^{-1}, due to the vibrational modes of anatase B1g, A1g + B1g, and Eg, respectively [28], whereas no peaks related to a different crystalline structure (i.e. brookite or rutile) were observed. In the case of USY-Ti catalyst, the vibration mode A1g + B1g of anatase overlaps with one vibration mode present in the USY at 520 cm^{-1}. These results, together with the above-mentioned comments on XRD spectra, suggest that TiO_2 is present in zeolites as small crystallites of anatase.

FT-IR spectra of some of the solids are shown in Fig. 2b. Our catalysts had the characteristic signals related to the zeolite structure; a wide signal at 3500 cm^{-1} (not shown) due to the hydroxyl groups (Brönsted acid) of the zeolite, a band at ca. 1600 cm^{-1} related to water absorbed in the internal zeolite framework, as well as several bands at 837, 793, 620, 530,

460 y 400 cm^{-1} [29]. However, it was not observed a significant increase in the shoulder appearing at 960 cm^{-1} in the systems where TiO_2 was incorporated. Ti–O–Si vibrations are reported to appear in this region [29]. These results seem to suggest that titanium has not been incorporated into the zeolitic structure, but small TiO_2 crystallites were deposited on the zeolite surface.

UV–Vis reflectance spectra of the USY-Ti-XXX systems are shown in Fig. 3. The formation of TiO_2 on the zeolite resulted in a blue-shift in the absorption spectrum of the TiO_2 and an increase in the band gap values (Table 1) of our catalysts compared to anatase TiO_2 [30] or the TiO_2-Pt catalyst prepared from commercial TiO_2 (P25 Degussa). Such a shift to a shorter wavelength in the absorption of TiO_2 can be attributed to the size quantization effect due to the presence of titania particles smaller than 10 nm [31]. The band gap of the USY-Ti catalyst was barely affected by the subsequent modification with the metals (Pt, Ag, Au), as can be seen in table 1. Nevertheless, the incorporation of Pt, Ag, or Au resulted in the extension of light absorption to the visible region (400-700 nm). USY-Ti-PAu and USY-Ti-IAu had a purple color, and they exhibited an absorption peak at 523 nm which was produced by the surface plasmon resonance (spr) of the metallic gold [32], which may have a positive effect in the photocatalytic production of H_2 [33,34]. In the case of the Pt systems, the absorption of visible radiation could be ascribed to the presence of PtO [35], whereas the absorption can be ascribed to the presence of Ag_2O in the case of the Ag systems [36].

BET surface and pore volume of the catalysts are shown in table 1. USY had a surface area and a cumulative pore volume of 691 m^2/g and 0.33 cm^3/g, respectively. The incorporation of TiO_2 and metal resulted in a small decrease in both parameters. The decrease was ca. 10-

30% and did not affect the type of N_2 isotherm (type II with H4 hysteresis) as can be seen in the N_2 isotherms in the supplementary information. Therefore, the structure of the zeolite was preserved, which was in agreement with the experimental results of XRD, FTIR, and Raman.

TEM and SEM pictures of the Pt-containing samples are shown in Fig.4. The characteristic morphology of the zeolite was maintained after the incorporation of TiO_2 and Pt (similar results were obtained for Ag and Au containing zeolites). The majority of the TiO_2 particles deposited on zeolite surface had a homogenous and small size of ca. 5-10 nm. This particle size was in agreement with the XRD and UV-visible results. Regarding platinum particles, their size (as evidenced by TEM) is also in the 5-10 nm range. EDX results (supplementary information), confirmed a good dispersion of both Ti and Pt in the samples. Moreover, the morphology of TiO_2 in USY-Ti-IPt and USY-Ti-PPt catalysts was maintained after the photocatalytic reaction, as can be seen in Fig.4c and Fig.4f. This suggests that the zeolite could stabilize the supported TiO_2.

The titanium content of our samples was analyzed by ICP-MS (Table 1). The amount of TiO_2 deposited on the zeolite was as expected, ca. 12% w/w, in all our catalysts. The noble metal content of our samples was studied by X-ray fluorescence analyses. Both methods, impregnation and photodeposition, led to similar metal content.

3.2. Photocatalytic production of hydrogen

The stoichiometry of glycerol total photoreforming can be described as follows:

$$C_3H_8O_3 + 3H_2O \rightarrow 3CO_2 + 7H_2 \quad (1)$$

Therefore, complete reforming of glycerol seems a simple reaction and would result in H_2/CO_2 ratio of 2.33. Nevertheless, according to the literature, the reaction could proceed through three different parallel reaction pathways involving an initial oxidation of primary or secondary carbons, or oxidative C-C scission [37]. In this sense, the higher the extent of the first two routes, the purer the hydrogen in the gas phase. The pathway, and therefore, the H_2/CO_2 ratio produced on glycerol photoreforming depend on the photocatalyst, glycerol concentration, and the experimental ratio is alike to the stoichiometry ratio when the glycerol conversion is high [38].

The zeolites were tested for hydrogen production through glycerol photoreforming and the global production of H_2 and CO_2 under UV radiation and solar-simulated radiation is shown in Fig.5a and Fig.5b, respectively. Not modified USY was not active in the photoreforming of glycerol 10% v/v, whereas all the TiO_2-containing zeolites were active in this reaction. Under our experimental conditions, glycerol conversion was pretty low, ca. 1%. As for the influence of the metal co-catalyst, the activity of the zeolitic photocatalysts decreased in the order Pt > Au > Ag under both UV and solar-simulated radiation, independently of the deposition procedure. This trend is similar to that obtained by other researchers for the photoreforming of oxygenated compounds with TiO_2-metal systems [39,40], and these results can be explained considering the work functions of the metals involved, Pt 5.7eV > Au 5.4 eV > Ag 4.6 eV [41].

For each specific metal (Pt, Au, Ag), the catalysts prepared by photodeposition had a higher H_2 production compared to the catalysts prepared by impregnation. The increase in the catalytic activity was small for USY-Ti-PAu and USY-Ti-PAg but higher for USY-Ti-PPt.

Since USY-Ti-IPt and USY-Ti-PPt had a similar structure, as it was observed by SEM, TEM, and XRD, the higher catalytic activity of the photodeposited catalyst could be related to the selective deposition of Pt on TiO_2 surface instead of the zeolite, since the photodeposition procedure requires the absorption of photons by the semiconductor [42]. In summary, H_2 produced with UV and solar-simulated radiation followed the same activity order: USY-Ti-PPt > USY-Ti-IPt > USY-Ti-PAu > USY-Ti-IAu > USY-Ti-PAg> USY-Ti-IPt, being Pt better than Au and Ag, and photodepositon better than impregnation.

Nevertheless, all zeolitic catalysts exhibited a H_2 production lower than TiO_2-Pt, the reference catalyst prepared by photodeposition, at the same catalyst concentration ($1g_{cat}/L$).

Comparing photocatalytic activity of TiO_2-Pt and the most active zeolitic system (USY-Ti-PPt), results are more similar under UV radiation than under solar-simulated light. Therefore, hydrogen productions of 18.0 mmol or 12.2 mmol (t = 16h) under UV light and 22.7 μmol or 5.1μ (t = 3h) under solar simulated light, for TiO_2-Pt and USY-Ti-Pt, respectively, were obtained.

The general loss on photocatalytic activity observed for the zeolitic catalysts with solar-simulated radiation compared to UV radiation can be explained by the blue-shift in the absorption spectrum of zeolite-supported TiO_2 compared to unsupported TiO_2 (Fig.3), and the increase in the band gap values (Table 1).

It is worth mentioning that the amount of TiO_2 was seven times lower in the zeolite-TiO_2 composite compared to TiO_2-Pt. Therefore, an additional experiment on a physical mixture of USY62 and TiO_2-Pt at the same Ti/zeolite ratio (9 mg TiO_2-Pt + 56 mg USY62) was

296 performed. As can be seen in Fig. 5a, the photocatalytic production of H_2 of diluted TiO_2-Pt
297 was almost six times lower (3.3 mmol) than the one obtained with not diluted TiO_2-Pt (18.0
298 mmol), being the activity loss proportional to the mass reduction. Dilution of TiO_2-Pt with
299 USY62 did not affect the inner photocatalytic activity of TiO_2-Pt, since an additional
300 experiment without USY62 (9 mg TiO_2-Pt) was performed and the photocatalytic activity of
301 9 mg TiO_2-Pt was similar to the physical mixture of 9 mg TiO_2-Pt and 56 mg of USY62.
302 Therefore, TiO_2 on USY-Ti-PPt was up to 4 times more active than unsupported TiO_2 on
303 glycerol photoreforming and supporting TiO_2 on USY62 had a beneficial effect on the
304 photocatalytic activity of TiO_2.

305 H_2 and CO_2 reaction rates, and H_2/CO_2 ratio of the catalysts under UV radiation at different
306 times (0.5, 1, 4, 8, and 16 h) are shown in Fig. 6. As far as the USY-Ti-XXX catalysts are
307 concerned, they had a similar trend in H_2 and CO_2 reaction rates. On one hand, H_2 reaction
308 rate was maximum at the beginning (0.5 h), and the rate hardly decreased during the
309 photoreforming for USY-Ti, USY-Ti-IPt, USY-Ti-PAu, USY-Ti-IAu, USY-Ti-PAg, and
310 USY-Ti-IPt catalysts (ca. 0-20 %), whereas the decrease was higher for USY-Ti-PPt (ca.
311 45 %). On the other hand, CO_2 reaction rate continuously increased during the 16 h of
312 reaction for all the USY-Ti-XXX catalysts. Thus, the CO_2 reaction rate after 16 h of reaction
313 was 2-5 times higher than the initial rate (0.5 h). All in all, the small CO_2 reaction rate at the
314 beginning of the reaction combined with the stable H_2 reaction rate produced H_2 with an
315 elevated purity in the gas phase (90-95% H_2 and 5-10% CO_2) during the first few hours of
316 reaction.

TiO_2-Pt had a different behavior compared to the zeolitic catalysts. H_2 and CO_2 reaction rates were maximum at the beginning (0.5 h), but it had a big deactivation after 16 h of reaction, 67% and 22%, respectively. This different behavior from that shown by the USY-Ti-XXX systems suggests that supporting TiO_2 on zeolite (USY62) not only increases the activity of TiO_2 (per gram of TiO_2) on glycerol photoreforming but also affects the catalytic behavior of the TiO_2. Since all the USY-Ti-XXX systems, regardless of the metal and deposition procedure used, had a similar trend in H_2 and CO_2 production rates, the different behavior seems to be produced by the dispersion of TiO_2 on zeolite surface or an interaction zeolite-TiO_2.

All in all, zeolite-supported TiO_2 (USY-Ti-PPt) was up to 4 times more active (per gram of TiO_2) than unsupported TiO_2 on glycerol photoreforming. However, it was challenging to know the precise nature of the zeolite-TiO_2 interaction when USY62 was the only zeolitic support used in the preparation of the composites. In brief, this could be a common interaction of the zeolite-TiO_2 systems, or it could require some specific properties in the zeolitic support (structure, surface area, ratio Si/Al, acidity, etc) to get this modification in the catalytic activity. It would be interesting to continue this investigation with the preparation of more Zeolite-TiO_2 composites with different zeolites and Zeolite-TiO_2 mass proportion. However, this falls beyond the scope of this study.

4. Conclusions

The results obtained in this work show that homogeneously dispersed TiO_2 (anatase) nanoparticles of ca. 10 nm on USY62, keeping the structure of the zeolite, can be prepared by sol-gel method. The small size of TiO_2 was confirmed by XRD, SEM, Raman, and FT-IR

spectroscopies, and the decrease of crystallite size is probably to account for the observed blue-shift in UV–vis spectra of zeolite-supported TiO_2 and the different photocatalytic behavior compared to unsupported TiO_2. As for the influence of the metal co-catalyst, the activity of the zeolitic photocatalysts decreased in the order Pt > Au > Ag with UV and solar-simulated radiation, which can be explained considering the work functions of the metals involved, Pt 5.7eV > Au 5.4 eV > Ag 4.6 eV. All Zeolite-supported systems had a smaller deactivation in H_2 production compared to unsupported TiO_2-Pt, being USY-Ti-PPt up to four times more active (per gram of TiO_2) than unsupported TiO_2 (TiO_2-Pt) on glycerol photoreforming.

Acknowledgements

The authors are thankful to MICIIN Grant NR: PID2019-104953RB-100, the Consejería de Transformación Económica, Industria, Conocimiento y Universidades de la Junta de Andalucía (UCO-FEDER Project CATOLIVAL, Ref. 1264113-R, 2018 call and Project Ref. P18-RT-4822) and FEDER Funds for Programa Operativo Fondo Social Europeo (FSE) de Andalucía 2014-2020 (DOC_01546).

References

[1] S.E. Hosseini, M.A. Wahid, Hydrogen production from renewable and sustainable energy resources: Promising green energy carrier for clean development, Renew. Sustain. Energy Rev. 57 (2016) 850–866. https://doi.org/10.1016/j.rser.2015.12.112.

[2] K. Chandrasekhar, Y.J. Lee, D.W. Lee, Biohydrogen production: Strategies to improve process efficiency through microbial routes, Int. J. Mol. Sci. 16 (2015) 8266–

8293. https://doi.org/10.3390/ijms16048266.

[3] T. Suganya, M. Varman, H.H. Masjuki, S. Renganathan, Macroalgae and microalgae as a potential source for commercial applications along with biofuels production: A biorefinery approach, Renew. Sustain. Energy Rev. 55 (2016) 909–941. https://doi.org/10.1016/j.rser.2015.11.026.

[4] A.R.K. Gollakota, N. Kishore, S. Gu, A review on hydrothermal liquefaction of biomass, Renew. Sustain. Energy Rev. 81 (2018) 1378–1392. https://doi.org/https://doi.org/10.1016/j.rser.2017.05.178.

[5] F.J. López-Tenllado, J. Hidalgo-Carrillo, V. Montes-Jiménez, E. Sánchez-López, F.J. Urbano, A. Marinas, Photocatalytic production of hydrogen from binary mixtures of C-3 alcohols on Pt/TiO_2 : Influence of alcohol structure, Catal. Today. 328 (2019) 2–7. https://doi.org/10.1016/j.cattod.2018.10.001.

[6] X. Jiang, X. Fu, L. Zhang, S. Meng, S. Chen, Photocatalytic reforming of glycerol for H 2 evolution on Pt/TiO_2: fundamental understanding the effect of co-catalyst Pt and the Pt deposition route, J. Mater. Chem. A. 3 (2015) 2271–2282.

[7] V. Kumaravel, S. Mathew, J. Bartlett, S.C. Pillai, Photocatalytic hydrogen production using metal doped TiO_2: A review of recent advances, Appl. Catal. B Environ. 244 (2019) 1021–1064. https://doi.org/https://doi.org/10.1016/j.apcatb.2018.11.080.

[8] R. Qian, H. Zong, J. Schneider, G. Zhou, T. Zhao, Y. Li, J. Yang, D.W. Bahnemann, J.H. Pan, Charge carrier trapping, recombination and transfer during TiO_2 photocatalysis: An overview, Catal. Today. 335 (2019) 78–90.

https://doi.org/10.1016/j.cattod.2018.10.053.

[9] G. Hu, J. Yang, X. Duan, R. Farnood, C. Yang, J. Yang, W. Liu, Q. Liu, Recent developments and challenges in zeolite-based composite photocatalysts for environmental applications, Chem. Eng. J. 417 (2021) 129209. https://doi.org/https://doi.org/10.1016/j.cej.2021.129209.

[10] M. Ge, J. Cai, J. Iocozzia, C. Cao, J. Huang, X. Zhang, J. Shen, S. Wang, S. Zhang, K.-Q. Zhang, Y. Lai, Z. Lin, A review of TiO_2 nanostructured catalysts for sustainable H_2 generation, Int. J. Hydrogen Energy. 42 (2017) 8418–8449. https://doi.org/https://doi.org/10.1016/j.ijhydene.2016.12.052.

[11] K. Czelej, J.C. Colmenares, K. Jabłczyńska, K. Ćwieka, Ł. Werner, L. Gradoń, Sustainable hydrogen production by plasmonic thermophotocatalysis, Catal. Today. 380 (2021) 156–186. https://doi.org/https://doi.org/10.1016/j.cattod.2021.02.004.

[12] L.M. Al-Harbi, S.A. Kosa, I.H. Abd El Maksod, E.Z. Hegazy, The Photocatalytic Activity of TiO_2-Zeolite Composite for Degradation of Dye Using Synthetic UV and Jeddah Sunlight, J. Nanomater. 2015 (2015) 565849. https://doi.org/10.1155/2015/565849.

[13] S. Hashimoto, Zeolites as single electron donors for photoinduced electron transfer reactions of guest aromatic species Diffuse reflectance laser photolysis study, J. Chem. Soc. Faraday Trans. 93 (1997) 4401–4408. https://doi.org/10.1039/A704955B.

[14] S. Suárez, I. Jansson, B. Ohtani, B. Sánchez, From titania nanoparticles to decahedral anatase particles: Photocatalytic activity of TiO_2/zeolite hybrids for VOCs oxidation,

Catal. Today. 326 (2019) 2–7. https://doi.org/https://doi.org/10.1016/j.cattod.2018.09.004.

[15] Z. Lv, Y. Tao, W. Zhang, Titanium dioxide supported on HZSM-5 for acid red 1 photocatalytic degradation, React. Kinet. Mech. Catal. 133 (2021) 531–539. https://doi.org/10.1007/s11144-021-01971-4.

[16] G. Liao, W. He, Y. He, Investigation of Microstructure and Photocatalytic Performance of a Modified Zeolite Supported Nanocrystal TiO_2 Composite, Catalysts. 9 (2019). https://doi.org/10.3390/catal9060502.

[17] I. Jansson, K. Yoshiiri, H. Hori, F.J. García-García, S. Rojas, B. Sánchez, B. Ohtani, S. Suárez, Visible light responsive Zeolite/WO_3–Pt hybrid photocatalysts for degradation of pollutants in air, Appl. Catal. A Gen. 521 (2016) 208–219. https://doi.org/https://doi.org/10.1016/j.apcata.2015.12.015.

[18] R.P. Nippes, D. Frederichi, e M.H.N. Olsen Scaliante, Enhanced photocatalytic performance under solar radiation of ZnO through hetero-junction with iron functionalized zeolite, J. Photochem. Photobiol. A Chem. 418 (2021) 113373. https://doi.org/https://doi.org/10.1016/j.jphotochem.2021.113373.

[19] Z. Razavi, N. Mirghaffari, A.A. Alemrajabi, F. Davar, M. Soleimani, Adsorption and photocatalytic removal of SO_2 using natural and synthetic zeolites-supported TiO_2 in a solar parabolic trough collector, J. Clean. Prod. 310 (2021) 127376. https://doi.org/https://doi.org/10.1016/j.jclepro.2021.127376.

[20] K. Guesh, C. Márquez-Álvarez, Y. Chebude, I. Díaz, Enhanced photocatalytic activity

of supported TiO_2 by selective surface modification of zeolite Y, Appl. Surf. Sci. 378 (2016) 473–478. https://doi.org/https://doi.org/10.1016/j.apsusc.2016.04.029.

[21] G. Zhang, A. Song, Y. Duan, S. Zheng, Enhanced photocatalytic activity of TiO_2/zeolite composite for abatement of pollutants, Microporous Mesoporous Mater. 255 (2018) 61–68. https://doi.org/https://doi.org/10.1016/j.micromeso.2017.07.028.

[22] J.C. Colmenares, A. Magdziarz, Room temperature versatile conversion of biomass-derived compounds by means of supported TiO_2 photocatalysts, J. Mol. Catal. A Chem. 366 (2013) 156–162. https://doi.org/https://doi.org/10.1016/j.molcata.2012.09.018.

[23] K. Roongraung, S. Chuangchote, N. Laosiripojana, Enhancement of Photocatalytic Oxidation of Glucose to Value-Added Chemicals on TiO_2 Photocatalysts by A Zeolite (Type Y) Support and Metal Loading, Catalysts. 10 (2020). https://doi.org/10.3390/catal10040423.

[24] N. Dubey, N.K. Labhsetwar, S. Devotta, S.S. Rayalu, Hydrogen evolution by water splitting using novel composite zeolite-based photocatalyst, Catal. Today. 129 (2007) 428–434. https://doi.org/https://doi.org/10.1016/j.cattod.2006.09.041.

[25] A. Taheri Najafabadi, F. Taghipour, Physicochemical impact of zeolites as the support for photocatalytic hydrogen production using solar-activated TiO_2-based nanoparticles, Energy Convers. Manag. 82 (2014) 106–113. https://doi.org/https://doi.org/10.1016/j.enconman.2014.03.003.

[26] A. Chang, W.-S. Peng, I.-T. Tsai, L.-F. Chiang, C.-M. Yang, Efficient hydrogen

production by selective alcohol photoreforming on plasmonic photocatalyst comprising sandwiched Au nanodisks and TiO_2, Appl. Catal. B Environ. 255 (2019) 117773. https://doi.org/https://doi.org/10.1016/j.apcatb.2019.117773.

[27] Z. Yan, D. Ma, J. Zhuang, X. Liu, X. Liu, X. Han, X. Bao, F. Chang, L. Xu, Z. Liu, On the acid-dealumination of USY zeolite: a solid state NMR investigation, J. Mol. Catal. A Chem. 194 (2003) 153–167. https://doi.org/https://doi.org/10.1016/S1381-1169(02)00531-9.

[28] W.F. Zhang, Y.L. He, M.S. Zhang, Z. Yin, Q. Chen, Raman scattering study on anatase TiO_2nanocrystals, J. Phys. D. Appl. Phys. 33 (2000) 912–916. https://doi.org/10.1088/0022-3727/33/8/305.

[29] M. Kang, W.-J. Hong, M.-S. Park, Synthesis of high concentration titanium-incorporated nanoporous silicates (Ti-NPS) and their photocatalytic performance for toluene oxidation, Appl. Catal. B Environ. 53 (2004) 195–205. https://doi.org/https://doi.org/10.1016/j.apcatb.2004.05.018.

[30] Z. He, Q. Cai, H. Fang, G. Situ, J. Qiu, S. Song, J. Chen, Photocatalytic activity of TiO_2 containing anatase nanoparticles and rutile nanoflower structure consisting of nanorods, J. Environ. Sci. 25 (2013) 2460–2468. https://doi.org/https://doi.org/10.1016/S1001-0742(12)60318-0.

[31] M. Anpo, M. Takeuchi, The design and development of highly reactive titanium oxide photocatalysts operating under visible light irradiation, J. Catal. 216 (2003) 505–516. https://doi.org/https://doi.org/10.1016/S0021-9517(02)00104-5.

[32] A. Tanaka, S. Sakaguchi, K. Hashimoto, H. Kominami, Preparation of Au/TiO_2 with metal cocatalysts exhibiting strong surface plasmon resonance effective for photoinduced hydrogen formation under irradiation of visible light, ACS Catal. 3 (2013) 79–85. https://doi.org/10.1021/cs3006499.

[33] K. Ćwieka, K. Czelej, J.C. Colmenares, K. Jabłczyńska, Ł. Werner, L. Gradoń, Supported Plasmonic Nanocatalysts for Hydrogen Production by Wet and Dry Photoreforming of Biomass and Biogas Derived Compounds: Recent Progress and Future Perspectives, ChemCatChem. 13 (2021) 1–40. https://doi.org/https://doi.org/10.1002/cctc.202101006.

[34] V. Nair, M.J. Muñoz-Batista, M. Fernández-García, R. Luque, J.C. Colmenares, Thermo-Photocatalysis: Environmental and Energy Applications, ChemSusChem. 12 (2019) 2098–2116. https://doi.org/https://doi.org/10.1002/cssc.201900175.

[35] H. Wang, Z. Wu, Y. Liu, Y. Wang, Influences of various Pt dopants over surface platinized TiO_2 on the photocatalytic oxidation of nitric oxide, Chemosphere. 74 (2009) 773–778. https://doi.org/https://doi.org/10.1016/j.chemosphere.2008.10.032.

[36] W. Zhou, H. Liu, J. Wang, D. Liu, G. Du, J. Cui, Ag_2O/TiO_2 Nanobelts Heterostructure with Enhanced Ultraviolet and Visible Photocatalytic Activity, ACS Appl. Mater. Interfaces. 2 (2010) 2385–2392. https://doi.org/10.1021/am100394x.

[37] K.E. Sanwald, T.F. Berto, W. Eisenreich, O.Y. Gutiérrez, J.A. Lercher, Catalytic routes and oxidation mechanisms in photoreforming of polyols, J. Catal. 344 (2016) 806–816. https://doi.org/10.1016/j.jcat.2016.08.009.

[38] X. Fu, X. Wang, D.Y.C. Leung, Q. Gu, S. Chen, H. Huang, Photocatalytic reforming of C3-polyols for H_2 production: Part (I). Role of their OH groups, Appl. Catal. B Environ. 106 (2011) 681–688. https://doi.org/https://doi.org/10.1016/j.apcatb.2011.05.045.

[39] K. Mogyorósi, Á. Kmetykó, N. Czirbus, G. Veréb, P. Sipos, A. Dombi, Comparison of the substrate dependent performance of Pt-, Au- and Ag-doped TiO_2 photocatalysts in H_2-production and in decomposition of various organics, React. Kinet. Catal. Lett. 98 (2009) 215. https://doi.org/10.1007/s11144-009-0052-y.

[40] N.T. Nguyen, S. Ozkan, O. Tomanec, X. Zhou, R. Zboril, P. Schmuki, Nanoporous AuPt and AuPtAg alloy co-catalysts formed by dewetting–dealloying on an ordered TiO_2 nanotube surface lead to significantly enhanced photocatalytic H_2 generation, J. Mater. Chem. A. 6 (2018) 13599–13606. https://doi.org/10.1039/C8TA04495C.

[41] H.L. Skriver, N.M. Rosengaard, Surface energy and work function of elemental metals, Phys. Rev. B. 46 (1992) 7157–7168. https://doi.org/10.1103/PhysRevB.46.7157.

[42] K. Wenderich, G. Mul, Methods, Mechanism, and Applications of Photodeposition in Photocatalysis: A Review, Chem. Rev. 116 (2016) 14587–14619. https://doi.org/10.1021/acs.chemrev.6b00327.

506 **Table 1.** Chemical composition, band gap, surface area and pore volume of the systems
507 prepared in the present work

508

Catalyst	ICP-MS	XRF	Band Gap	S_{BET}	Pore Volume
	$\%TiO_2$ (w/w)	% Metal (w/w)	(eV)	m^2/g	cm^3/g
USY	---	---	---	691	0.33
USY-Ti	14.4	---	3.45	569	0.34
USY-Ti-PPt	12.0	0.71	3.48	580	0.23
USY-Ti-IPt	12.0	1.19	3.49	609	0.25
USY-Ti-PAg	12.0	0.91	3.39	565	0.25
USY-Ti-IAg	12.0	0.75	3.41	581	0.28
USY-Ti-PAu	12.0	2.86	3.54	462	0.21
USY-Ti-IAu	12.8	2.97	3.44	561	0.26
TiO_2-Pt	99.56	0.44	3.19	56	0.23

509

510

Figure 1. XRD patterns of the zeolitic catalysts.

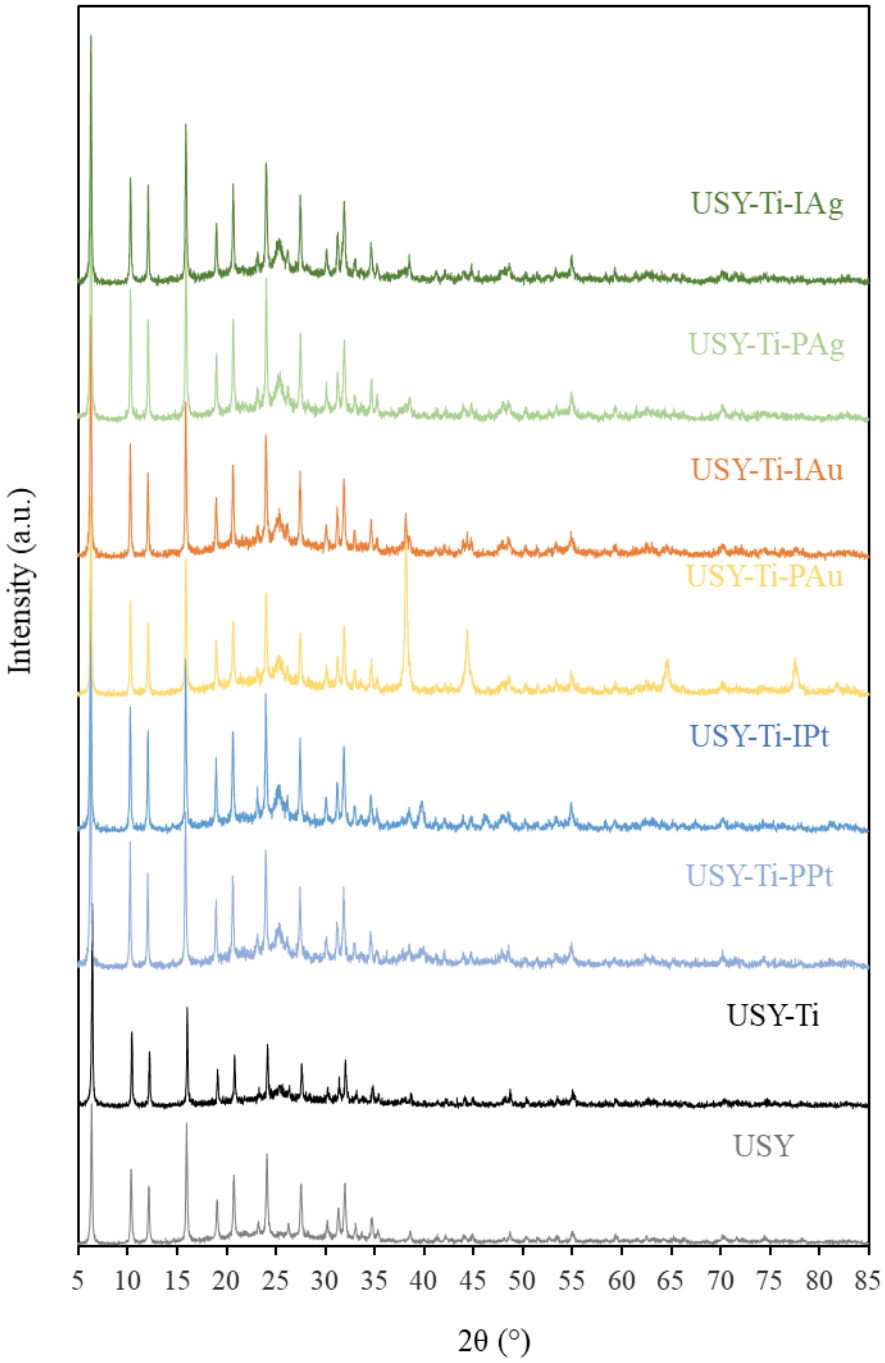

514 **Figure 2.** Raman (a) and FTIR (b) spectra of some of the catalysts.

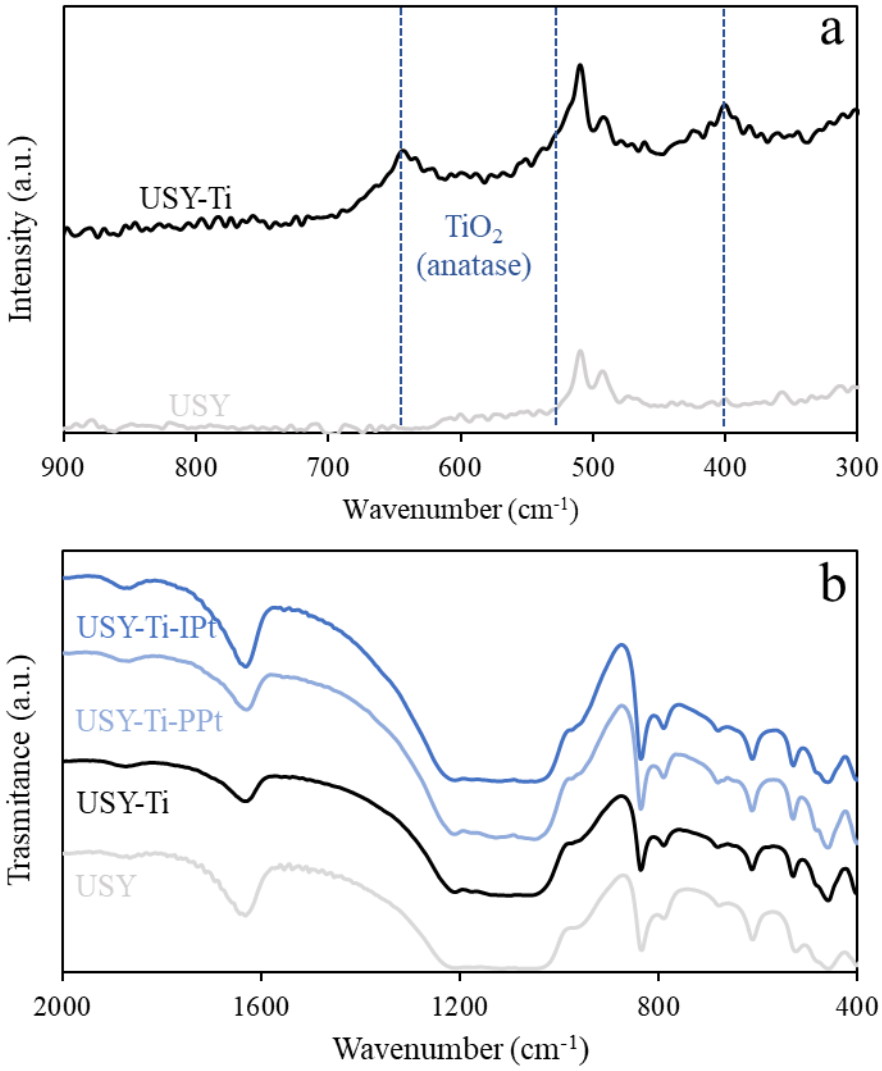

515

516

517

518

519

Figure 3. UV-visible spectra of the TiO_2-containing catalysts.

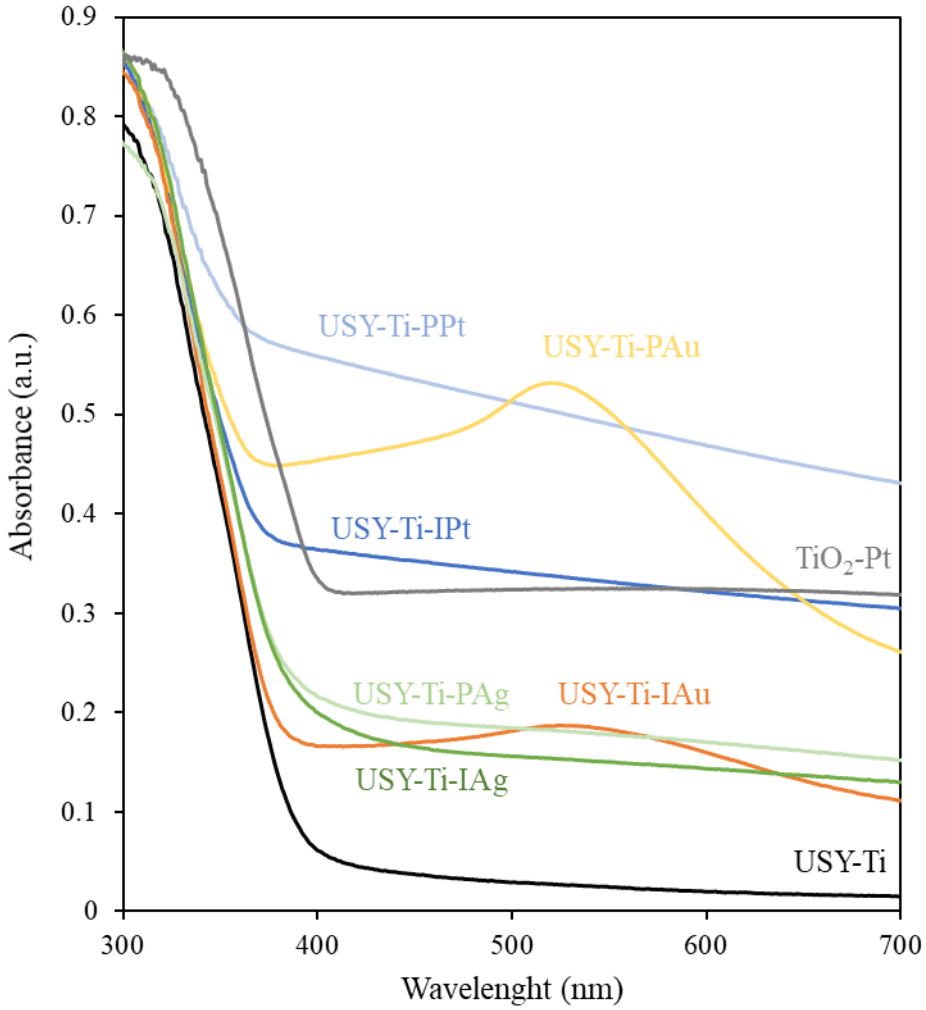

Figure 4. TEM micrograph of USY-Ti-PPt (a) and USY-Ti-IPt (d), and SEM micrograph of USY-Ti-PPt (b fresh, c used) and USY-Ti-IPt (e fresh, f used).

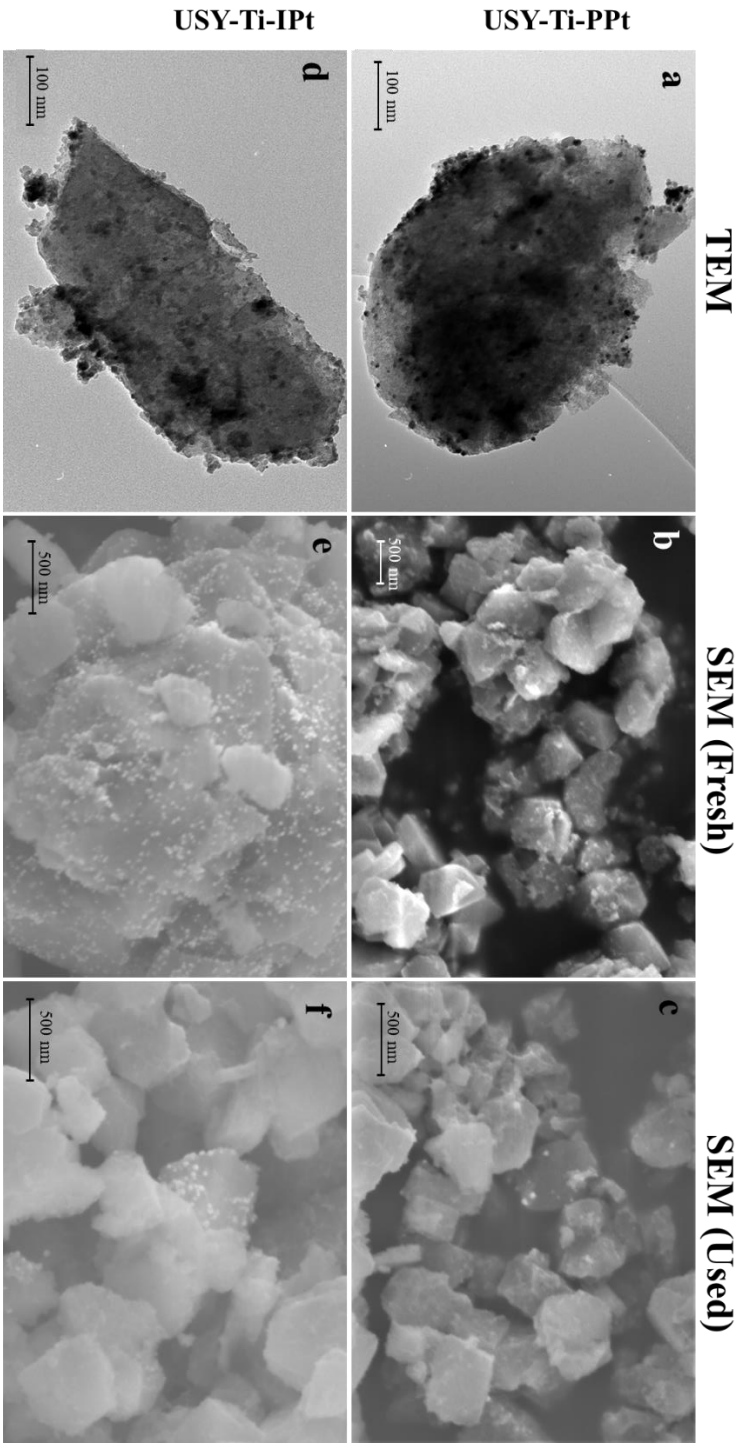

Figure 5. Photocatalytic production of H_2 and CO_2 on the different catalysts under UV radiation and 16 h (a) or solar-simulated radiation and 3 h (b). Results found for a physical mixture of USY and TiO_2-Pt (86:14 w/w) have also been included for the sake of comparison.

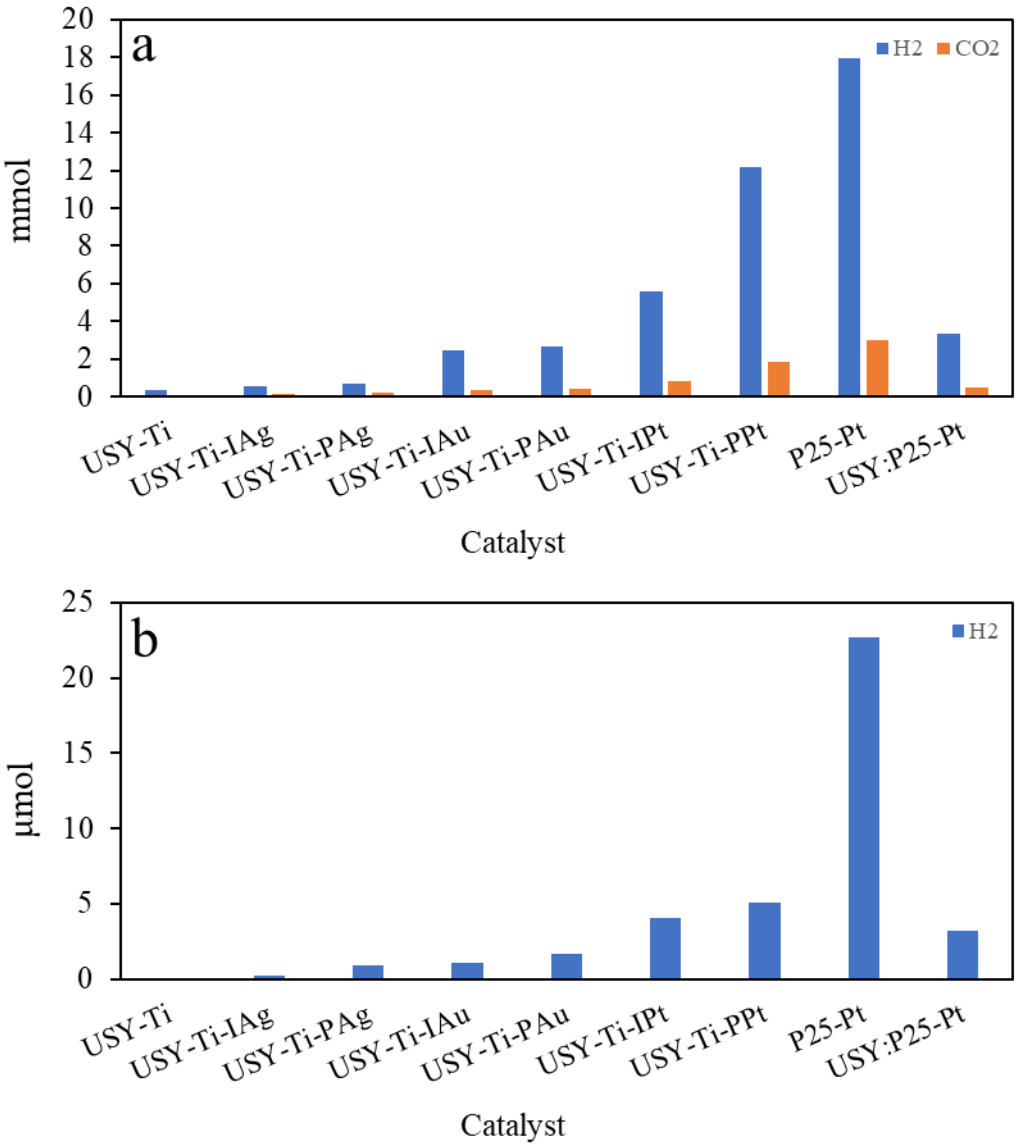

Figure 6. H_2 (a) and CO_2 (b) photoproduction, and H_2/CO_2 ratio (C) on the different catalysts under UV at different reaction times. Results found for a physical mixture of USY and TiO_2-Pt (86:14 w/w) have also been included for the sake of comparison.